

Probing the QCD Critical Point with Higher Moments of Net-proton Multiplicity Distributions

Xiaofeng Luo for the STAR Collaboration

Department of Modern Physics, University of Science and Technology of China, Hefei 230026, China

Nuclear Science Division, Lawrence Berkeley National Laboratory, Berkeley, CA 94720, USA

E-mail: xfluo@lbl.gov

Abstract. Higher moments of event-by-event net-proton multiplicity distributions are applied to search for the QCD critical point in the heavy ion collisions. It has been demonstrated that higher moments as well as moment products are sensitive to the correlation length and directly connected to the thermodynamic susceptibilities computed in the Lattice QCD and Hadron Resonance Gas (HRG) model. In this paper, we will present measurements for kurtosis (κ), skewness (S) and variance (σ^2) of net-proton multiplicity distributions at the mid-rapidity ($|y| < 0.5$) and $0.4 < p_T < 0.8$ GeV/ c for Au+Au collisions at $\sqrt{s_{NN}}=19.6, 39, 62.4, 130$ and 200 GeV, Cu+Cu collisions at $\sqrt{s_{NN}}=22.4, 62.4$ and 200 GeV, d+Au collisions at $\sqrt{s_{NN}}=200$ GeV and p+p collisions at $\sqrt{s_{NN}}=62.4$ and 200 GeV. The moment products $\kappa\sigma^2$ and $S\sigma$ of net-proton distributions, which are related to volume independent baryon number susceptibility ratio, are compared to the Lattice QCD and HRG model calculations. The $\kappa\sigma^2$ and $S\sigma$ of net-proton distributions are consistent with Lattice QCD and HRG model calculations at high energy, which support the thermalization of the colliding system. Deviations of $\kappa\sigma^2$ and $S\sigma$ for the Au+Au collisions at low energies from HRG model calculations are also observed.

1. Introduction

One of the main goals of heavy ion collision is to explore the phase structure of hot, dense nuclear matter [1]. Finite temperature Lattice QCD calculations demonstrate that with vanishing baryon chemical potential ($\mu_B = 0$), the phase transition from the hadronic phase to the Quark Gluon Plasma (QGP) phase is a smooth crossover [2]. The corresponding transition temperature is about 170 – 190 MeV [3, 4]. At large μ_B region, the phase transition between hadronic phase and QGP phase is of first order [5] and with a second order end point at the boundary towards the crossover region, which is so called QCD Critical Point (CP) [6]. Although many efforts have been made by theorist and experimentalist to search for the CP, its location or even the existence is still not confirmed yet [7]. The first principle Lattice QCD calculation at finite μ_B are difficult due to the fermion sign problem. Several techniques, such as Re-weighting, Image baryon chemical potential and Taylor expansion [8] *etc.*, have been developed to overcome those problems and make the Lattice QCD calculable at finite μ_B region. However, large uncertainties are still there.

Experimentally, heavy ion collision provides us a good opportunity to search for the CP. To access the QCD phase diagram, we can tune the chemical freeze out temperature (T) and baryon chemical potential (μ_B) by varying the colliding energy. As the characteristic signatures of the

CP in a static and infinite medium is the divergence of the correlation length (ξ) and increase of non-Gaussian fluctuations. Thus, non-monotonic signals of CP are expected to be observed if the evolution trajectory (T, μ_B) in the QCD phase diagram of the system pass nearby the critical region and the signals are not washed out by the expansion of the colliding system.

Due to the finite size effect, rapid expansion and critical slowing down *etc.*, the typical correlation length (ξ) developed in the heavy ion collision near the QCD critical point is a small value about 2 – 3 fm [9]. Recently, model calculations reveal that higher moments of conserved quantities distributions are proportional to the higher power of the correlation length [10, 11], such as fourth order cumulant $\langle (\delta N)^4 \rangle - 3 \langle (\delta N)^2 \rangle^2 \sim \xi^7$, where $\delta N = N - M$, N is the particle multiplicity in one event and M is the averaged particle multiplicity of the event sample. On the other hand, the higher moments as well as moment products of conserved quantities distributions are also directly connected to the corresponding susceptibilities in Lattice QCD [12, 13] and HRG model [14] calculations, for e.g. the third order susceptibility of baryon number ($\chi_B^{(3)}$) is related to the third cumulant ($\langle (\delta N_B)^3 \rangle$) of baryon number distributions as $\chi_B^{(3)} = \langle (\delta N_B)^3 \rangle / VT^3$; V, T are volume and temperature of system respectively. It has been found that the volume independence baryon number susceptibility ratio can be directly connected to the moment products of baryon number distributions as $\kappa\sigma^2 = \chi_B^{(4)} / \chi_B^{(2)}$ and $S\sigma = \chi_B^{(3)} / \chi_B^{(2)}$, which allows us to compare the theoretical calculations with experimental measurements. Theoretical calculations also demonstrate that the experimental measurable net-proton number (proton minus anti-proton number) event-by-event fluctuations can reflect the baryon number and charge fluctuations [15]. Thus, higher moments of the net-proton multiplicity distributions are applied to search for the QCD critical point in the heavy ion collisions [16, 17, 18]. When approaching the QCD critical point, the moment products $\kappa\sigma^2$ and $S\sigma$ will show large deviation from its Poisson statistical value. The skewness is expected to change its sign when system evolution trajectory in the phase diagram cross phase boundary [19].

In year 2010, RHIC Beam Energy Scan (BES) program [20] was carried out to map the first order QCD phase boundary and search for the QCD critical point by tuning the colliding energy from 39 GeV down to 7.7 GeV with the corresponding μ_B coverage about 100 – 410 MeV. With the large uniform acceptance and good capability of particle identification STAR detector, it provides us very good opportunities to find the QCD critical point with sensitive observable, if the existence of QCD critical point is true.

2. Experimental Method

The data presented in the paper are obtained using the Solenoidal Tracker at RHIC (STAR). Those are Au+Au collisions at $\sqrt{s_{NN}}=19.6$ (year 2001), 39, 62.4 (year 2004), 130 and 200 GeV (year 2004), Cu+Cu collisions at $\sqrt{s_{NN}}=22.4, 62.4, 200$ GeV, d+Au at $\sqrt{s_{NN}}=200$ GeV (year 2003) and p+p collisions at $\sqrt{s_{NN}}=62.4$ (year 2006), 200 GeV (year 2009). The main subsystem used in this analysis is a large, uniform acceptance cylindrical Time Projection Chamber (TPC) covering a pseudo-rapidity range of $|\eta| < 1$ and 2π azimuthal coverage. As a primary tracking device, it can measure the trajectories and momenta of particles with transverse momenta above 0.15 GeV/ c . To ensure the purity and similar efficiency, the protons and anti-protons are identified with the ionization energy loss (dE/dx) measured by TPC of STAR detector within $0.4 < p_T < 0.8$ GeV/ c and mid-rapidity ($|y| < 0.5$). Several track quality cuts are also used to select the tracks with good quality in each event. We require the distance of closest approach (dca) to the primary vertex of proton (antiproton) track less than 1 cm to suppress the contamination from secondary protons (antiproton). To study the centrality dependence of higher moments, centralities are determined by the uncorrected charged particle multiplicities ($dN_{ch}/d\eta$) within pseudo-rapidity $|\eta| < 0.5$ measured by TPC. By comparing measured $dN_{ch}/d\eta$ with the Monte Carlo Glauber model results, we can obtain the average

number of participant N_{part} , impact parameter b and number of binary nucleon-nucleon collisions N_{bin} for each centrality class.

3. Analysis Method

In this section, we will introduce you how to perform the higher moments analysis with experimental data. First, we will show you the definition of the cumulants and various moments used in our analysis, such as standard deviation (σ), skewness (S) and kurtosis (κ). Then, we will discuss about the *Centrality Bin Width Effect* (CBWE).

3.1. Moments and Cumulants of Event-by-Event Fluctuations

In statistics, probability distribution functions can be characterized by the various moments, such as mean (M), variance (σ^2), skewness (S) and kurtosis (κ). Before introducing the above moments used in our analysis, we would like to define cumulants, which are alternative methods to the moments of a distribution. The cumulants determine the moments in the sense that any two probability distributions whose cumulants are identical will have identical moments as well.

Experimentally, we measure net-proton number event-by-event wise, $N_{p-\bar{p}} = N_p - N_{\bar{p}}$, which is proton number minus antiproton number, in the mid-rapidity ($|y| < 0.5$) and within the transverse momentum $0.4 < p_T < 0.8$ GeV/ c . In the following, we use N to represent the net-proton number $N_{p-\bar{p}}$ in one event. The average value over whole event ensemble is denoted by $\langle N \rangle$, where the single angle brackets are used to indicate ensemble average of an event-by-event distributions.

The deviation of N from its mean value are defined by

$$\delta N = N - \langle N \rangle. \quad (1)$$

Then, we can define the various order cumulants of event-by-event distributions as:

$$C_{1,N} = \langle N \rangle, C_{2,N} = \langle (\delta N)^2 \rangle, C_{3,N} = \langle (\delta N)^3 \rangle, C_{4,N} = \langle (\delta N)^4 \rangle - 3 \langle (\delta N)^2 \rangle^2. \quad (2)$$

An important property of the cumulants is their additivity for independent variables. If X and Y are two independent random variables, then we have $C_{i,X+Y} = C_{i,X} + C_{i,Y}$ for i th order cumulant. This property will be used in our study.

Once we have the definition of cumulants, various moments can be denoted as:

$$M = C_{1,N}, \sigma^2 = C_{2,N}, S = \frac{C_{3,N}}{(C_{2,N})^{3/2}}, \kappa = \frac{C_{4,N}}{(C_{2,N})^2} \quad (3)$$

And also, the moments product $\kappa\sigma^2$ and $S\sigma$ can be expressed in term of cumulant ratio.

$$\kappa\sigma^2 = \frac{C_{4,N}}{C_{2,N}}, S\sigma = \frac{C_{3,N}}{C_{2,N}}. \quad (4)$$

With above definition of various moments, we can calculate various moments and moment products with the measured event-by-event net-proton fluctuations for each centrality.

3.2. Centrality Bin Width Effect (CBWE) Correction

The centralities in this analysis are determined by the uncorrected charged particle multiplicity (N_{ch}) measured at middle pseudo-rapidity ($|\eta| < 0.5$) by the TPC of the STAR detector. Before calculating various moments of net-proton distributions for one centrality, such as 0–5%, 5–10%, we should consider the so called *Centrality Bin Width Effect* (CBWE) arising from the impact

parameter fluctuations due to the finite centrality bin width. This effect must be corrected, as it may cause different centrality dependence. To formulate and demonstrate the centrality bin width effect, we write the event-by-event net-proton distributions in one centrality:

$$P(N) = \sum_i \omega_i f^{(i)}(N), (\sum_i \omega_i = 1), \quad (5)$$

where the ω_i and $f^{(i)}(N)$ are the weighted and net-proton distributions for i th impact parameter in one centrality, respectively. From eqs. (2)-(5) and (11), we can calculate the various order cumulants for the distribution $P(N)$ as below:

$$C_{1,N} = \sum_i \omega_i C_{1,N}^i = \sum_i \omega_i \langle N \rangle_i \quad (6)$$

$$C_{2,N} = (\sum_i \omega_i C_{2,N}^i) + C'_{2,C_{1,N}^i} \quad (7)$$

$$C_{3,N} = (\sum_i \omega_i C_{3,N}^i) + C'_{3,C_{1,N}^i} + 3 \times C'_{1,C_{1,N}^i,1,C_{2,N}^i} \quad (8)$$

$$\begin{aligned} C_{4,N} = & (\sum_i \omega_i C_{4,N}^i) + C'_{4,C_{1,N}^i} + 4 \times C'_{1,C_{1,N}^i,1,C_{3,N}^i} \\ & + 6 \times C'_{1,(C_{1,N}^i)^2,1,C_{2,N}^i} - 12 \times (C'_{1,C_{1,N}^i})(C'_{1,C_{1,N}^i,1,C_{2,N}^i}) \\ & - 3 \times (C'_{2,C_{1,N}^i})^2 + 3 \times C'_{2,C_{2,N}^i}, \end{aligned} \quad (9)$$

where the $C_{k,N}^i$ ($k = 1, 2, 3, 4$) are the k^{th} order cumulant for net-proton distribution $f^{(i)}(N)$; the $C'_{k,X}$ ($X = C_{m,N}^i$, $k, m = 1, 2, 3, 4$) are k^{th} order cutmulant for random variable $X = C_{m,N}^i$ under the discrete probability distribution $Prob(X) = \omega_i$; the $C'_{1,X,1,Y} = \langle XY \rangle - \langle X \rangle \langle Y \rangle$ ($X = C_{k,N}^i$, $k = 1, 2, 3, 4$) are the first order joint cumulant for random variable X, Y under the discrete probability distribution $Prob(X, Y) = \omega_i$. We find that the higher order cumulants $C_{k,N}$ ($k = 1, 2, 3, 4$) can be expressed by the addition of two parts, one is the weighted average of the same order cumulant of each sub-distribution $f^{(i)}(N)$, and the other part is the cumulant of lower order cumulant under the discrete weighted distributions, which stems from the fluctuation of impact parameters within the centrality and results in the CBWE.

Experimentally, the smallest centrality bin is determined by a single uncorrected reference multiplicity value measured by TPC. Generally, we usually report our results for a wider centrality bin, such as 0–5%, 5–10%, ...etc., to suppress the statistical fluctuations. To eliminate the centrality bin width effect, we calculate the various moment for each single N_{ch} within one wider centrality bin and weighted averaged by the number of events in each N_{ch} .

$$\sigma = \frac{\sum_r n_r \sigma_r}{\sum_r n_r} = \sum_r \omega_r \sigma_r, \quad (10)$$

$$S = \frac{\sum_r n_r S_r}{\sum_r n_r} = \sum_r \omega_r S_r, \quad (11)$$

$$\kappa = \frac{\sum_r n_r \kappa_r}{\sum_r n_r} = \sum_r \omega_r \kappa_r, \quad (12)$$

where the n_r is the number of events in r^{th} refmult and the corresponding weight $\omega_r = n_r / \sum_r n_r$.

4. Results

In this section, we will present beam energy and system size dependence for the various moments (M, σ, S, κ) as well as moment products ($\kappa\sigma^2, S\sigma$) of net-proton distributions for Au+Au collisions at $\sqrt{s_{NN}} = 19.6, 39, 62.4, 130, 200$ GeV, Cu+Cu collisions at $\sqrt{s_{NN}} = 22.4, 62.4, 200$ GeV, d+Au collisions at $\sqrt{s_{NN}} = 200$ GeV and p+p collisions at $\sqrt{s_{NN}} = 62.4, 200$ GeV. First, we will show the typical event-by-event net-proton multiplicity distributions from different colliding systems. Then we studied the centrality as well as energy dependence of various moments and moment products. The systematic errors are estimated by varying the following requirements for $p(\bar{p})$ tracks: DCA, track quality reflected by the number of ot points used in track reconstruction and the dE/dx selection criteria for $p(\bar{p})$ identification. The statistical and systematic error are shown separately by lines and brackets, respectively.

4.1. Event-by-Event Net-proton Multiplicity Distributions

Event-by-event net-proton multiplicity distributions for Au+Au collisions at $\sqrt{s_{NN}} = 39$ GeV measured within $0.4 < p_T < 0.8$ GeV/c and $|y| < 0.5$ are shown in Fig. 1. Going from peripheral to central collisions, it is found that the distributions become wider and more symmetric for central collisions.

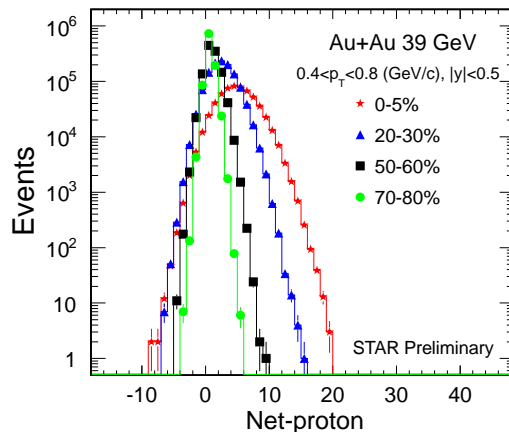


Figure 1. Typical event-by-event net-proton multiplicity distributions for Au+Au collisions at $\sqrt{s_{NN}} = 39$ GeV.

4.2. Centrality Dependence of Moments and Moment Products of Net-proton Distributions

The centrality (N_{part}) dependence for various moments (M, σ, S, κ) of net-proton multiplicity distributions from Au+Au collisions at $\sqrt{s_{NN}}=39, 62.4$ and 200 GeV, Cu+Cu collisions at $\sqrt{s_{NN}}=22.4, 62.4$ and 200 GeV, d+Au collisions at $\sqrt{s_{NN}}=200$ GeV and p+p collisions at $\sqrt{s_{NN}}=62.4$ and 200 GeV are shown in Fig. 2 and Fig. 3. We find that M and σ increase with N_{part} monotonically, while S and κ decrease with N_{part} . The centrality and energy dependence of S and κ indicate that the net-proton distributions become more symmetric for more central collision and higher energies.

The dashed lines in the Fig. 2 and Fig. 3 represent the expectations from Central Limit Theorem (CLT) when assuming the superposition of many identical and independent particle emission sources in the system [17, 18]. In Fig. 2 and 3, the centrality dependence of various moments can be well described by the dashed lines expected from CLT. Especially in Fig. 3, the various moments of p+p and d+Au collisions follow the CLT lines of Cu+Cu collision at the

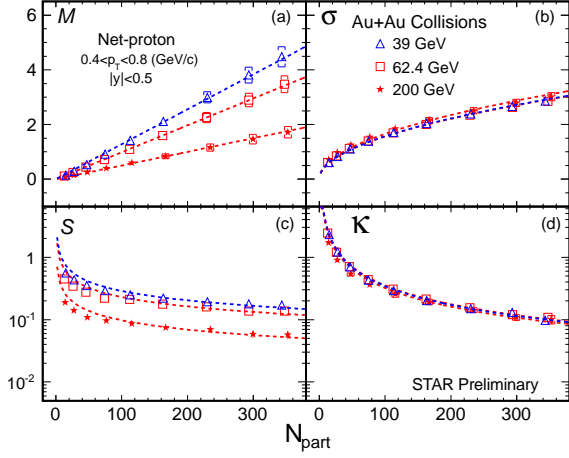


Figure 2. Centrality dependence of various moments of net-proton multiplicity distributions for Au+Au collisions at $\sqrt{s_{NN}} = 39, 62.4, 200$ GeV. The dashed lines shown in the figure are expectation lines from Central Limit Theorem (CLT).

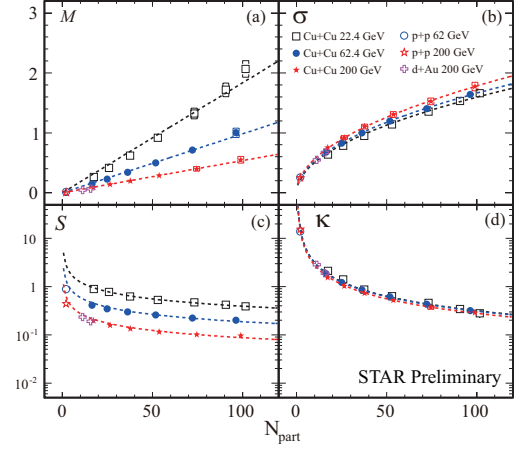


Figure 3. Centrality dependence of various moments of net-proton multiplicity distributions for Cu+Cu collisions at $\sqrt{s_{NN}} = 22.4, 62.4$ and 200 GeV, d+Au collisions at $\sqrt{s_{NN}} = 200$ GeV and p+p collisions at $\sqrt{s_{NN}} = 62.4$ and 200 GeV. The dashed lines shown in the figure are expectation lines from Central Limit Theorem (CLT).

corresponding energy very well. This also supports the identical independent emission sources assumption. Fig. 4 shows the centrality dependence of moment products $S\sigma$ and $\kappa\sigma^2$ of net-

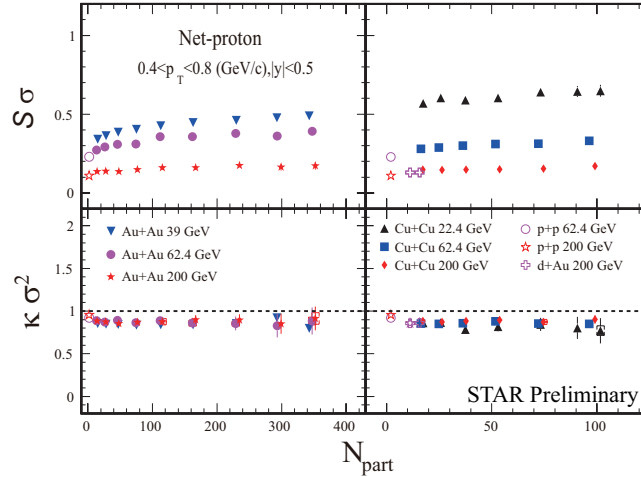


Figure 4. Moment products ($\kappa\sigma^2$ and $S\sigma$) of net-proton distributions for Au+Au, Cu+Cu, d+Au and p+p collisions.

proton distributions, which are directly related to the baryon number susceptibility ratio in Lattice QCD and HRG models as $\kappa\sigma^2 = \chi_B^{(4)}/\chi_B^{(2)}$ and $S\sigma = \chi_B^{(3)}/\chi_B^{(2)}$, for p+p, Cu+Cu and Au+Au collisions at various colliding energies. $S\sigma$ shows a weak increase with centrality, while the $\kappa\sigma^2$ shows no centrality dependence.

4.3. Energy Dependence of the Moment Products ($S\sigma$ and $\kappa\sigma^2$)

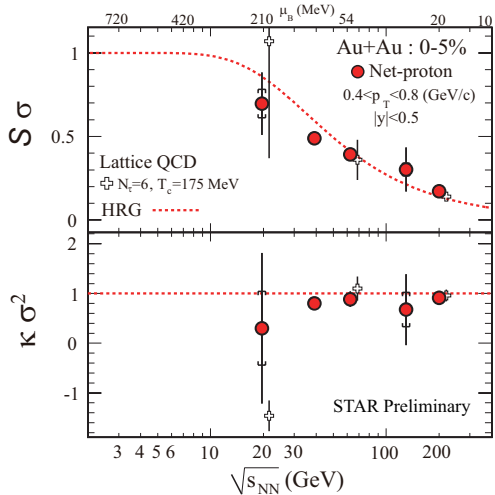


Figure 5. Energy dependence of moment products ($\kappa\sigma^2$ and $S\sigma$) of net-proton distributions for central Au+Au collisions (0 – 5%, 19.6 GeV: 0 – 10%, 130 GeV: 0 – 6%). The red dashed lines denote the HRG model calculations, in which the $S\sigma = \tanh(\mu_B/T)$ and $\kappa\sigma^2=1$. The empty markers denote the results calculated from Lattice QCD [4].

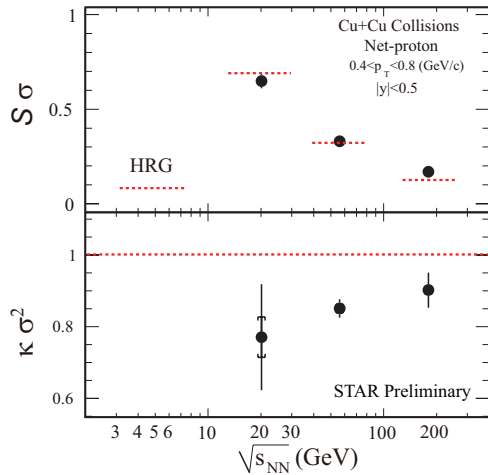


Figure 6. Energy dependence of moment products ($\kappa\sigma^2$ and $S\sigma$) of net-proton distributions for Cu+Cu central collisions (0 – 10%, 22.4 GeV: 0 – 5%). The dashed lines shown in the figures are from HRG model calculations, in which $S\sigma = \tanh(\mu_B/T)$ and $\kappa\sigma^2=1$. The μ_B and T values are taken from [21].

In Fig. 5, we show the energy dependence of the $S\sigma$ and $\kappa\sigma^2$ of net-proton distributions for most central Au+Au collisions (0 – 5%, 19.6 GeV: 0 – 10%, 130 GeV: 0 – 6%). Lattice QCD [4] and HRG model [14] calculations are also shown for comparison. Lattice QCD results are obtained with time extent $N_\tau = 6$ and phase transition temperature at $\mu_B=0$, $T_c = 175$ MeV. The red dashed lines of the HRG model in the upper panel and lower panels are evaluated by $S\sigma = \tanh(\mu_B/T)$ and $\kappa\sigma^2 = 1$, respectively, where the μ_B/T ratio at chemical freeze-out is parameterized as a function of colliding energy based on reference [22]. The corresponding baryon chemical potential (μ_B) at chemical freeze-out for each energy is shown in the upper band of the Fig. 5. We find that the moment products ($\kappa\sigma^2$ and $S\sigma$) of Au+Au collisions at $\sqrt{s_{NN}}=200, 130, 62.4$ GeV are consistent with Lattice QCD and HRG model calculations. The $S\sigma$ and $\kappa\sigma^2$ for Au+Au collisions at $\sqrt{s_{NN}} = 39$ GeV deviates from HRG model calculations. Surprisingly, $\kappa\sigma^2$ from Lattice QCD calculations at $\sqrt{s_{NN}} = 19.6$ GeV show a negative value [4]. However, due to the limited statistics, the statistical errors of experimental data are large at 19.6 GeV. The STAR is running to take more data at 19.6 GeV in year 2011. Those deviations could be linked to the chiral phase transition [23] and presence of QCD critical point [24]. Recent linear σ model calculations demonstrate that the fourth order cumulant of the fluctuations for σ field will be universally negative, when the QCD critical point is approached from cross-over side [24]. It will cause the measured $\kappa\sigma^2$ as well as kurtosis (κ) of net-proton distributions to be smaller than their Poisson expectation values.

Fig. 6 shows the energy dependence of $\kappa\sigma^2$ and $S\sigma$ for Cu+Cu central collisions. The red dashed lines in the figure are obtained from the HRG model by using the formula $S\sigma = \tanh(\mu_B/T)$, where the μ_B and T are from thermal model fits of the particle ratios. We find that our experimental data is consistent with HRG model expectations for $S\sigma$ of net-proton distributions. While the $\kappa\sigma^2$ deviates from HRG model calculations and monotonically

decrease as the collision energy decreases.

4.4. Charged Particle Density ($dN_{ch}/d\eta$) Scaling of $S\sigma$ and Evidence of Thermalization in Heavy Ion Collisions

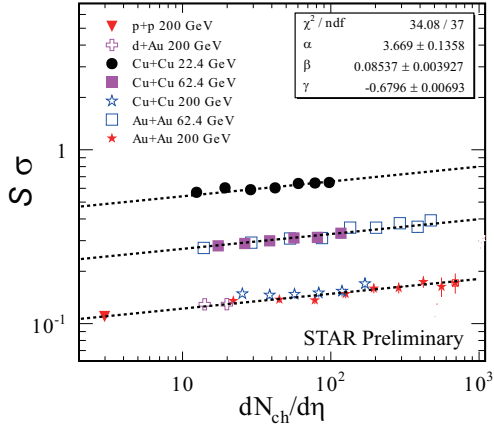


Figure 7. $S\sigma$ of net-proton distributions as a function of charged particle density at mid-rapidity ($dN_{ch}/d\eta$) for various colliding systems. The dashed lines in the figures is the fitting lines.

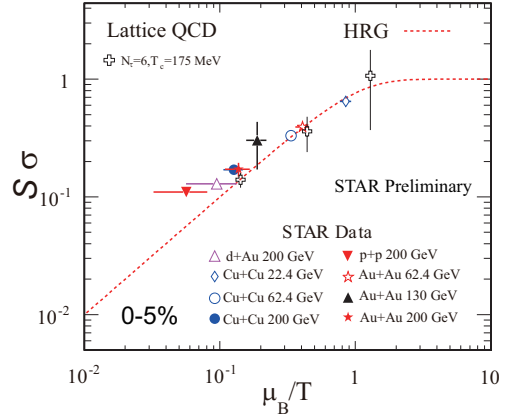


Figure 8. $S\sigma$ of net-proton distributions as a function of baryon chemical potential over temperature ratio (μ_B/T) for most central collisions (0–5%, 130 GeV: 0–6%, d+Au : 0–20%). The red dashed line in the figures is the result of the HRG model. Lattice QCD results with $N_\tau = 6$ and $T_c = 175$ MeV are also shown in the figure.

The $S\sigma$ of net-proton distributions for various colliding systems including Au+Au collisions at $\sqrt{s_{NN}} = 62.4$ and 200 GeV, Cu+Cu collisions at $\sqrt{s_{NN}} = 22.4$, 62.4 and 200 GeV, d+Au and p+p collisions at $\sqrt{s_{NN}} = 200$ GeV, as a function of $dN_{ch}/d\eta$ are shown in the Fig. 7 with double logarithm axis. It is obvious that for a fixed colliding energy, such as $\sqrt{s_{NN}}=200$ GeV, the moment products of $S\sigma$ of net-proton distributions for different system size the p+p, d+Au, Cu+Cu and Au+Au collisions have power law dependence on the charged particle density ($dN_{ch}/d\eta$). Thus, we fit the $S\sigma$ of net-proton distributions for various colliding systems with double power law formula:

$$S\sigma(dN_{ch}/d\eta, \sqrt{s_{NN}}) = \alpha \times (dN_{ch}/d\eta)^\beta \times (\sqrt{s_{NN}})^\gamma \quad (13)$$

The fitting results are shown in the Table. 1. The $S\sigma$ can be well described by the power law

Table 1. Fitting parameters for $S\sigma$ as a function of $dN_{ch}/d\eta$

Parameters	Value	Approx.
χ^2/ndf	34.08/37	0.92
α	3.669 ± 0.1358	$\frac{11}{3}$
β	0.0853 ± 0.003927	$\frac{1}{12}$
γ	-0.6796 ± 0.00693	$-\frac{2}{3}$

formula $S\sigma = \frac{11}{3} \times \left(\frac{1}{s^4} \frac{dN_{ch}}{d\eta}\right)^{\frac{1}{12}}$, where the s is the square of the center of mass energy. For high energy heavy ion collisions the temperature is approximately constant and the ratio $\mu_B/T \ll 1$,

thus we have the approximation $\mu_B/T \sim \tanh(\mu_B/T) = S\sigma = \frac{11}{3} \times (\frac{1}{s^4} \frac{dN_{ch}}{d\eta})^{\frac{1}{2}}$. This denotes the relation between μ_B/T and the charged particle density and colliding energy for high energy nuclear collisions.

Multiplicity fluctuations and inclusive yields are two basic properties in high energy heavy ion collisions. For a thermal system, both the fluctuations and yields should be described by the thermodynamic parameters (μ_B and T), which completely determine the properties of the thermal system. The fluctuation observable $S\sigma$ of most central net-proton distributions versus thermodynamic parameter μ_B/T ratios, which are extracted from the thermal model fit of the particle ratio, is shown in the Fig. 8 for various colliding systems. Lattice QCD calculations with $N_\tau = 6$ and $T_c = 175$ MeV and the HRG model relation $S\sigma = \tanh(\mu_B/T)$ are also plotted in Fig. 8 for comparison. We find that high energy heavy ion collisions, such as Au+Au and Cu+Cu collisions, are consistent with Lattice QCD and HRG model calculations, while the elementary p+p collision deviate from the HRG model calculations. In addition to the perfect description of the particle yields by the thermal model, the agreement of higher order fluctuations with thermal model predications provide further evidence that the colliding system has achieved thermalization in most central high energy heavy ion collision.

5. Summary

The higher moments of net-proton multiplicity distributions measured in heavy ion collision experiment have been applied to search for the QCD critical point, due to the high sensitivity to the correlation length (ξ). The beam energy and system size dependence for higher moments (M, σ, S, κ) as well as moment products ($\kappa\sigma^2, S\sigma$) of net-proton multiplicity distributions have been presented with a broad energy range and different system sizes, which include Au+Au collisions at $\sqrt{s_{NN}} = 200, 130, 62.4, 39$ and 19.6 GeV, Cu+Cu collisions at $\sqrt{s_{NN}} = 200, 62.4$ and 22.4 GeV, d+Au collisions at $\sqrt{s_{NN}} = 200$ GeV, p+p collisions at $\sqrt{s_{NN}} = 200$ and 62.4 GeV. The moment product $\kappa\sigma^2$ shows no centrality dependence while $S\sigma$ shows a weak centrality dependence. The energy dependence is studied by comparing the results from the Au+Au 200 GeV to those from the BES energies. The moment products $\kappa\sigma^2$ and $S\sigma$ of net-proton distributions from most central Au+Au collisions are consistent with Lattice QCD and HRG model calculations at high energy (200, 130, 62.4 GeV) while deviating from (smaller than) HRG model calculations at $\sqrt{s_{NN}} = 39$ GeV. Lattice QCD calculations show negative value for $\kappa\sigma^2$ at $\sqrt{s_{NN}} = 19.6$ GeV. The deviations could potentially be linked to chiral phase transitions and QCD critical point. But the experimental data is with large error bar due to the limited statistics. Fortunately, this ambiguity can be clarified soon by 19.6 GeV data taken in year 2011 with higher statistics. Recent model calculations show that the $\kappa\sigma^2$ value will always be smaller than its Poisson statistical value 1, when QCD critical point is approached from the high energy cross-over side.

On the other hand, the mutual agreements between the μ_B/T extracted from thermal model fits of particle ratio and from the event-by-event fluctuations observable $S\sigma$ of net-proton distributions provides further evidence of thermalization of the hot dense matter created in the heavy ion collisions. Further, the $\kappa\sigma^2$ and $S\sigma$ of net-proton distributions are consistent with Lattice QCD and HRG model calculations at high energy, which support the thermalization of the colliding system. The deviations of the $\kappa\sigma^2$ and $S\sigma$ of net-proton distributions for Au+Au central collisions from HRG model predications at low energies are not well understood. This may result from the non-applicability of grand canonical ensemble or the appearance of QCD critical point and chiral phase transitions at low energies. However, it should be further investigated.

Acknowledgement

We thank S. Gupta, F. Karsch, K. Rajagopal, K. Redlich, M. Stephanov for enlightening discussions. We thank the RHIC Operations Group and RCF at BNL, the NERSC Center at LBNL and the Open Science Grid consortium for providing resources and support. This work was supported in part by the Offices of NP and HEP within the U.S. DOE Office of Science, the U.S. NSF, the Sloan Foundation, the DFG cluster of excellence ‘Origin and Structure of the Universe’ of Germany, CNRS/IN2P3, FAPESP CNPq of Brazil, Ministry of Ed. and Sci. of the Russian Federation, NNSFC, CAS, MoST, and MoE of China, GA and MSMT of the Czech Republic, FOM and NWO of the Netherlands, DAE, DST, and CSIR of India, Polish Ministry of Sci. and Higher Ed., Korea Research Foundation, Ministry of Sci., Ed. and Sports of the Rep. Of Croatia, and RosAtom of Russia.

References

- [1] J. Adams *et al.* (STAR Collaboration), *Nucl. Phys. A* **757** (2005) 102.
- [2] Y. Aoki *et al.*, *Nature* **443** 675 (2006).
- [3] Y. Aoki *et al.*, *Phys. Lett. B* **643** (2006) 46; M. Cheng *et al.*, *Phys. Rev. D* **74** (2006) 054507.
- [4] S. Gupta, X. Luo, B. Mohanty, H. G. Ritter, N. Xu, arXiv: 1105.3934.
- [5] S. Ejiri, *Phys. Rev. D* **78** (2008) 074507 ; E. S. Bowman, J. I. Kapusta, *Phys. Rev. C* **79** (2009) 015202.
- [6] M. A. Stephanov, *Prog. Theor. Phys. Suppl.* **153** (2004) 139; Z. Fodor and S. D. Katz, *Journal of High Energy Physics* **0404** (2004) 50; R. V. Gavai, S. Gupta, *Phys. Rev. D* **78** (2008) 114503.
- [7] M. A. Stephanov, *Int. J. Mod. Phys. A* **20** (2005) 4387; B. Mohanty, *Nucl. Phys. A* **830** (2009) 899c.
- [8] Z. Fodor, S. D. Katz, *Phys. Lett. B* **534** (2002) 87; Philippe de Forcrand and O. Philipsen, *Nucl. Phys. B* **642** (2002) 290; R. V. Gavai, S. Gupta, *Phys. Rev. D* **68** (2003) 034506.
- [9] M. A. Stephanov *et al.*, *Phys. Rev. D* **60** (1999) 114028; B. Berdnikov and K. Rajagopal, *Phys. Rev. D* **65** (2000) 105017.
- [10] M. A. Stephanov, *Phys. Rev. Lett.* **102** (2009) 032301.
- [11] C. Athanasiou *et al.*, *Phys. Rev. D* **82** (2010) 074008.
- [12] R. V. Gavai and S. Gupta, *Phys. Lett. B* **696** (2011) 459.
- [13] M. Cheng, *et al.*, *Phys. Rev. D* **79** (2009) 074505.
- [14] F. Karsch and K. Redlich, *Phys. Lett. B* **695** (2011) 136.
- [15] Y. Hatta and M. A. Stephanov, *Phys. Rev. Lett.* **91** (2003) 102003.
- [16] X. Luo *et al.*, arXiv:1105.5049.
- [17] M. M. Aggarwal *et al.* (STAR Collaboration), *Phys. Rev. Lett.* **105** (2010) 022302.
- [18] X. Luo *et al.*, *J. Phys. G: Nucl. Phys.* **37** (2010) 094061.
- [19] M. Asakawa *et al.*, *Phys. Rev. Lett.* **103** (2009) 262301.
- [20] B. I. Abelev *et al.* (STAR Collaboration), *Phys. Rev. C* **81** (2010) 024911; STAR Internal Note - SN0493, 2009.
- [21] M. M. Aggarwal *et al.*, *Phys. Rev. C* **83** (2010) 34910.
- [22] J. Cleymans *et al.*, *Phys. Rev. C* **73** (2006) 034905.
- [23] B. Friman, arXiv:1103.3511.
- [24] M. A. Stephanov, arXiv:1104.1627.